# Vibrational Fault Diagnosis of Bearing in Rotating Machineries using Hilbert-Huang Transform (HHT)

Aman S. Chougule, Prof. Prasad Shinde
*Rajarambapu Institute of technology Islampur*

**Abstract: Rotating machinery depends on fault diagnosis for smooth operations and avoiding severe breakdowns. This study delves into detecting bearing faults by analyzing vibration signals using the Hilbert-Huang Transform (HHT). HHT stands out in handling the complex signals typical in rotating machinery due to its ability to deal with non-linear and non-stationary characteristics. The analysis starts with Empirical Mode Decomposition (EMD), which breaks down vibration signals into intrinsic mode functions (IMFs). These IMFs offer a detailed view of the signal's time-frequency features. By applying the Hilbert Transform to these IMFs, the method uncovers the instantaneous frequency and amplitude, enabling accurate fault detection. The main goal here is to improve the precision and dependability of bearing fault diagnosis using the unique strengths of HHT. This, in turn, aims to enhance maintenance practices and minimize downtime in industrial environments. The effectiveness of this approach is proven through comprehensive experiments and comparative studies, highlighting its success in identifying and categorizing various bearing faults.**

## 1-INTRODUCTION

Rotating machinery heavily relies on rolling element bearings to function smoothly with minimal friction. Unfortunately, these bearings are susceptible to premature failure due to errors in installation, lack of proper lubrication, or excessive loads. It is crucial to detect any issues early on to maintain product quality and prevent safety hazards or damage.

One of the primary methods used to identify faults in bearings is vibration analysis, which analyzes vibration signals to uncover any abnormalities. Techniques such as time-domain and frequency-domain analysis, the shock pulse method, and acoustic emission analysis are commonly utilized for diagnosing the condition of bearings. Vibrations are generated as flaws interact with rolling elements, producing pulses at distinct frequencies.

While the Fast Fourier Transform is a widely used tool in signal processing, it encounters challenges with high background noise and complex faults. Similarly, non-adaptive methods like the wavelet transform have difficulty handling noisy signals. This study introduces a fresh approach called the Hilbert-Huang Transform (HHT) for diagnosing bearing faults, specifically effective in capturing the complex and ever-changing vibrations in rotating machinery.

The process involves breaking down vibration signals into intrinsic mode functions (IMFs) using Empirical Mode Decomposition (EMD), followed by a detailed time-frequency analysis with the Hilbert Transform. EMD and similar methods have been increasingly utilized to identify faults in bearings, gears, and transformers. The aim is to enhance the accuracy and reliability of bearing fault diagnosis, assisting in proactive maintenance and minimizing unexpected downtime.

Through thorough experimental validation and a comparative study, this novel approach demonstrates its effectiveness, contributing to the advancement of diagnostic techniques for rotating machinery.

In order to thoroughly understand the current technologies available for bearing fault diagnosis, we conducted an extensive review of various existing studies and literature. The references we examined include a range of research papers, technical articles, and industry reports. These sources provided valuable insights into the methodologies, tools, and approaches currently being utilized in the field. Below is a comprehensive list of the references we have studied to inform our review:

[1]Zhang et al. proposed a quantitative technique for estimating the severity of faults in bearings in induction machines by reconstructing an airgap displacement profile from variations in mutual inductance, which was validated through simulations and experiments.

[2]Li H et al. developed an enhanced empirical mode decomposition (EMD) method using cubic trigonometric B-spline interpolation to analyze non-linear and non-stationary signals. This innovation

improved signal decomposition accuracy by reducing overshoot and undershoot issues compared to traditional methods, as supported by experimental outcomes.

[4]Zhang X. et al. introduced an optimized Time Varying Filtering based Empirical Mode Decomposition (TVF-EMD) method using the Grey Wolf Optimizer (GWO) for machinery fault diagnosis. With a weighted kurtosis index to refine decomposition parameters, the study enhanced frequency separation and noise robustness. Case studies and simulations confirmed the effectiveness of this approach in diagnosing faults in rotating machinery.

[5]Kankar P. et al. explored diagnosing ball bearing faults with localized defects through wavelet-based feature extraction. They utilized the Minimum Shannon Entropy Criterion to choose the Complex Morlet wavelet for statistical feature extraction from raw vibration data. By employing artificial intelligence techniques like SVM, LVQ, and SOM, they found that SVM outperformed the others in fault classification accuracy.

[6]Elbouchikhi E. et al. developed a technique for detecting bearing faults in induction machines by analyzing stator currents using the Hilbert-Huang transform. This method estimated intrinsic mode functions through empirical mode decomposition, which were further processed to identify fault signatures accurately. Simulations and experiments validated the method's efficacy in assessing fault severity based on the IMFs' IA and IF.

[7]Wang J. et al. presented the EMD manifold (EMDM) method as a noise-assisted technique to improve fault diagnosis in rotating machines by addressing mode mixing in empirical mode decomposition. This approach adaptively combines different fault-related modes to preserve true transients while minimizing interference from residual noise. Experimental results on gearbox and bearing faults demonstrated superior performance compared to traditional noise-assisted EMD methods.

[8]Yin C. et al. proposed a method for extracting subtle fault features in rolling bearings using improved ensemble noise-reconstructed empirical mode decomposition (IENEMD) and adaptive threshold denoising (ATD). This approach demonstrated superior performance in extracting weak fault features compared to existing methods, validated through simulations and real-world cases.

[10]Ricci R. et al. introduced a method for diagnosing gear faults using empirical mode decomposition (EMD) in combination with a merit index for automatically selecting intrinsic mode functions (IMFs) for the Hilbert-Huang spectrum. Their approach showed effectiveness in identifying faults under transient operational conditions through experimental trials on a spiral bevel gearbox.

[12]Marple L. presented frequency-domain algorithms for calculating complex-valued discrete-time "analytic" signals from real-valued N-point signals. These algorithms generated standard analytic signals and adjusted endpoints to ensure accuracy in the transformation process.

| Glossary of acronyms | |
|---|---|
| HHT | Hilbert-Huang transform |
| EMD | Empirical mode decomposition |
| IMF | Intrinsic mode function |
| FFT | Fast Fourier transform |
| CM | Condition monitoring |
| RMS | Root mean square |
| BPFO | Ball pass frequency outer |
| BPFI | Ball pass frequency inner |
| BSF | Ball spin frequency |
| FTF | Fundamental train frequency |

*Table 1. Acronyms.*

## 2-METHODOLOGY

This section provides a thorough explanation of the Hilbert-Huang Transform (HHT) methodology, which is essential for fault detection. It delves into the setup and functioning of the system used for acquiring and processing vibration signals. Additionally, the entire process, covering signal acquisition, processing, and analysis, is outlined.

### 2.1 – HILBERT – HUANG TRANSFORM (HHT):

The HHT is a sophisticated analytical method consisting of two key components: Empirical Mode Decomposition (EMD) and Hilbert Spectral Analysis. EMD is utilized to break down a complex signal into simpler intrinsic mode functions (IMFs).

Once the signal is decomposed into IMFs, Hilbert Spectral Analysis examines each mode to determine its complex envelope. This systematic approach enables a detailed and precise analysis of non-linear and non-stationary signals.

### 2.1.1- EMPIRICAL MODE DECOMPOSITION (EMD):

Empirical Mode Decomposition (EMD) is a method utilized to break down a signal into its Intrinsic Mode Functions (IMFs). IMFs, in this context, are representations of various oscillatory patterns within the signal and must adhere to two key conditions. The first condition (C1) stipulates that the number of local extreme points (both peaks and valleys) should either match the number of zero-crossings precisely or differ by just one. The second condition (C2) requires that the mean value of the envelope constructed from these local extreme points equals zero. These conditions serve to ensure that the signal exhibits symmetry, displaying positive peaks accompanied by negative valleys. Any signal can undergo decomposition through EMD, with the IMF criteria serving as a blueprint for the process. The breakdown process encompasses: 1. Detecting the extreme points within the input signal x(t). 2. Estimating the upper ($e_{max}$) and lower ($e_{min}$) envelopes based on cubic spline interpolation applied to the identified extreme points.

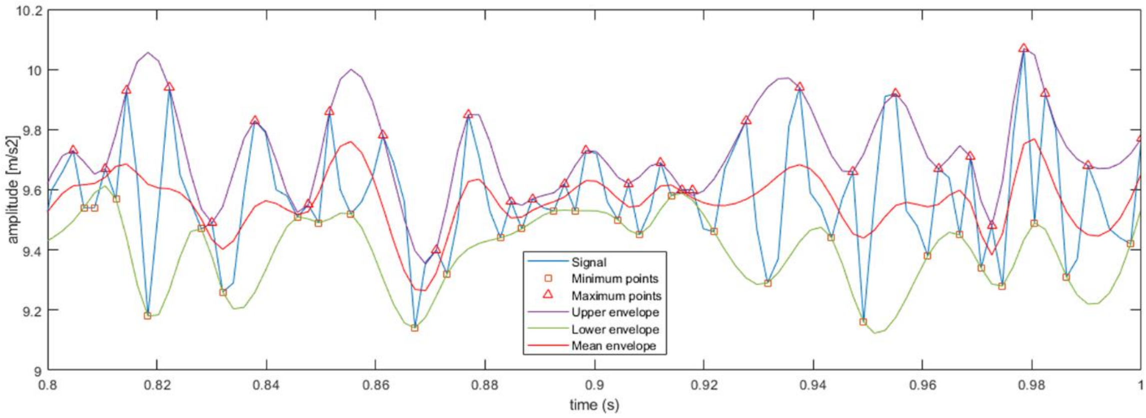


*Fig.1. Variables involved in the process of obtaining an EMD*

3. The Calculation of the mean ($m_1$) in between the upper and lower envelope.

$$m_1=(e_{min}(t) + e_{max}(t))/2 \qquad (1)$$

4. Subtraction of the average of the envelopes $m1$ to signal x(t) to obtain $h1$. This $h1$ is a proto-IMF, a possible IMF.

$$h_1(t) = x(t) - m_1(t) \qquad (2)$$

5.Once a proto-IMF is obtained, it is evaluated to determine if it meets conditions C1 and C2 to qualify as an IMF. If it does, the proto-IMF is considered an IMF. If not, the proto-IMF is treated as the new x(t), and the process of identifying extrema and interpolating envelopes is repeated. This iteration continues until the IMF conditions are met.

Achieving the C2 condition often requires numerous iterations. To ensure the physical significance of the IMFs in terms of frequency and amplitude modulations, a stopping criterion is essential. In this study, the iteration stops when the standard deviation (SD) between two consecutive proto-IMFs, as defined in equation (3), reaches 0.2. This threshold is chosen to prevent the IMF from stopping near the target frequency, which could lead to the splitting of relevant information across multiple modes.

$$SD = \sum_{t=0}^{T} \frac{|h_i(t) - h_{i-1}(t)|^2}{h_{i-1}^2(t)} \qquad (3)$$

6. Determination of the residual $r1$ which will be the difference between the original signal x(t) and the found IMF $hi(t)$.

$$r_1(t) = x(t) - hi(t) \qquad (4)$$

7. After separating the Intrinsic Mode Functions (IMFs), the remaining signal is analyzed. If the residual signal is either consistently increasing or decreasing or includes only three high and low points, the decomposition process stops because no more IMFs can be extracted. However, if the residual signal is not following a simple pattern, suggesting additional complexity, the decomposition process restarts from step 2 to isolate more IMFs.

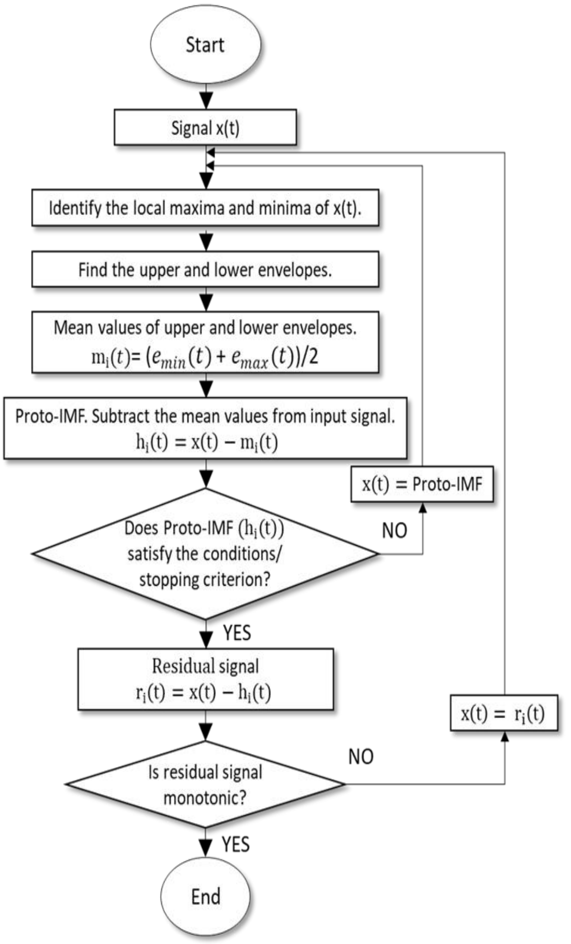


*Fig. 2. EMD flow diagram.*

Figure 1 depicts the essential elements necessary to derive an IMF, while Figure 2 outlines the flowchart of the Empirical Mode Decomposition (EMD) process, emphasizing the main and secondary loops. The primary loop, which determines when to end the decomposition of the signal, evaluates the trend of the residual signal. On the contrary, the secondary loop must satisfy conditions C1 and C2 to identify an IMF or meet the termination condition based on the standard deviation between adjacent data points to halt.

EMD's method of decomposing signals provides a straightforward visualization (Figure 1) of signal breakdown at every stage without depending on the Fourier transform. This direct method renders EMD adaptable and practical in various scenarios. Nonetheless, there are aspects of EMD that could be improved. One such aspect is the termination condition for signal decomposition, as the number of iterations required for a proto-IMF to develop into an IMF hinges on this condition. A surplus of iterations might complicate selecting the optimal IMF for analysis.

Another issue pertains to the envelope utilized to smooth the curve, which could introduce unintended peaks and troughs, resulting in new endpoints and distorting the signal. Furthermore, a challenge arises regarding the impact of the initial and final thresholds of the data sequence on the envelope, leading to unnecessary fluctuations when there are no additional data points to extend the envelope. The most significant challenge lies in mode mixing, where the algorithm encounters difficulty distinguishing various signal characteristics, merging them into a single IMF and complicating their identification.

2.1.2-HILBERT SPECTRAL ANALYSIS:

Once the signal has been broken down into its Intrinsic Mode (IMFs), the Hilbert transform (HT) is employed to determine the envelope function. The HT is a technique used to extract the envelope of a signal by considering the input data as complex numbers without any imaginary components. After applying the HT, the imaginary part values of the signal are calculated using equations (5 (6), and (7).

$$x_0 = fft(x_{input}) \qquad (5)$$

$$x_{an}(n) = \begin{cases} 2 * x_0(n), \ 1 < n < \frac{N}{2} - 1 \\ x_0, \ n = 0, \frac{N}{2} \\ 0, \ \frac{N}{2} + 1 < n < N - 1 \end{cases} \qquad (6)$$

$$x_b = ifft(x_{an^*} x_0) \qquad (7)$$

In equation (5), $xinput$ represents the input signal and $X0$ is the Fast Fourier Transform (FFT) of the input signal. Equation (6) computes $Xan$ as the analytical signal by multiplying the elements of $X0$ with the multiples derived from the three equations, where N signifies the total number of samples to process, and n is the sample being worked on ranging from 0 to N-1 [12]. In equation (7), the inverse Fourier transform of the product of X$an$ with $X0$ is found. Consequently, the resulting $xb$ includes the real part X$input$ and a calculated imaginary part, allowing for the inverse Fourier transform of the product of X$env$ as per:

$$Xenv = \sqrt{Xb.conjugada(Xb)} \qquad (8)$$

Finally, the frequency content of the envelope is extracted using the fast Fourier transform (9).

$$Xenvelope = |ff(xenv)| \qquad (9)$$

2.2.2.- CONFIGURATION AND CALIBRATION OF THE SYSTEM:

Prior to commencing any measurements on the experimental setup, it is necessary to calibrate the measurement system. This calibration procedure involves utilizing an industrial data acquisition system, a constant vibration calibrator for amplitude and frequency, and a vibration generator. Both the proposed measurement system and the acquisition system undergo calibration using a Bruel & Kjaer type 4294 vibration calibrator that emits a steady vibration signal at 159.2 Hz with an acceleration of 10 m/s² RMS. This allows for adjusting the amplitude gain of both systems accordingly. The acquisition system consists of a National Instruments PXI-4472B model and an IEPE monoaxial accelerometer from PCB Piezotronics model 352C65.

*Table 2. Type A precision and standard uncertainty result [13].*

| Measurements comparison | | |
|---|---|---|
| Frequency | Prototype [m/s²] | PXI-NI [m/s²] |
| 20 Hz | 12.71 | 12.34 |
| 25 Hz | 8.80 | 8.46 |
| 31.5 Hz | 10.94 | 10.51 |
| 40 Hz | 15.01 | 14.52 |
| 50 Hz | 7.68 | 7.31 |
| 63 Hz | 12.54 | 12.44 |
| 80 Hz | 10.89 | 10.43 |
| 100 Hz | 8.39 | 8.19 |
| 125 Hz | 14.53 | 14.33 |
| 160 Hz | 12.40 | 12.41 |
| 200 Hz | 6.04 | 6.46 |
| 250 Hz | 8.83 | 10.14 |
| 315 Hz | 5.92 | 8.49 |
| 400 Hz | 6.27 | 12.17 |
| 500 Hz | 4.84 | 10.31 |
| Standard uncertainty Type A | | |
| System | 160 Hz @12.4 m/s² | |
| PXI-NI | 0.001 | |
| Prototypo | 0.01 | |

Following calibration, simultaneous measurements of the vibration response are conducted using a Bruel & Kjaer type 4809 vibration generator with both the prototype system and the acquisition system. These measurements are taken at varying frequencies and amplitudes. Figure 4 displays the measurements of the nominal center frequencies of one-third octave (1/3 OB) at different frequencies up to 500 Hz obtained from both systems.

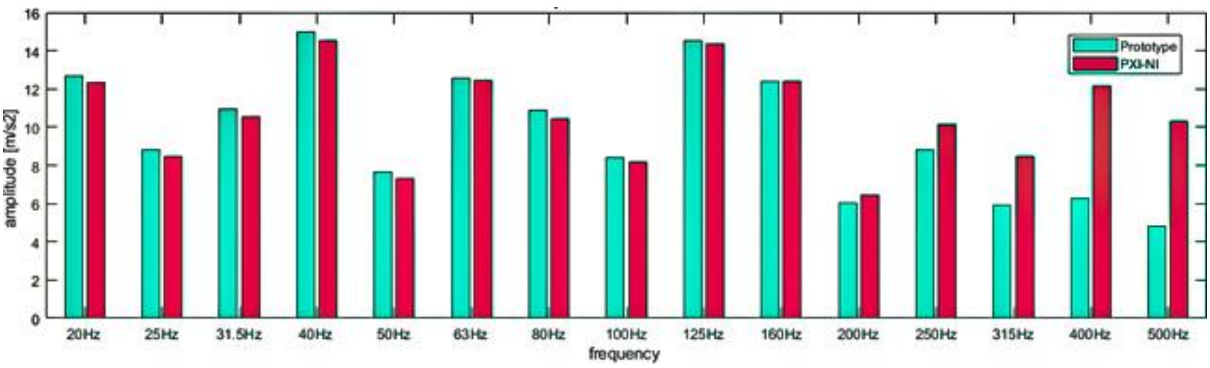


*Fig. 3. Vibration response at the center one-third octave frequencies of the prototype and with the PXI-NI acquisition system.*

To assess the standard uncertainty, 30 samples were taken for a signal at 160 Hz with an acceleration of 12.4 m/s² using both the prototype system and the acquisition system. The standard uncertainty values for the prototype system and the PXI-NI acquisition system were found to be quite similar. This similarity indicates that the prototype's measurements are reliable and can be compared to those from the commercial acquisition system within the appropriate bandwidth. A summary of the vibration response at nominal one-third octave center frequencies ranging from 20 to 500 Hz and the type A standard uncertainty is detailed in Table 2.

3-EXPERIMENTAL SETUP

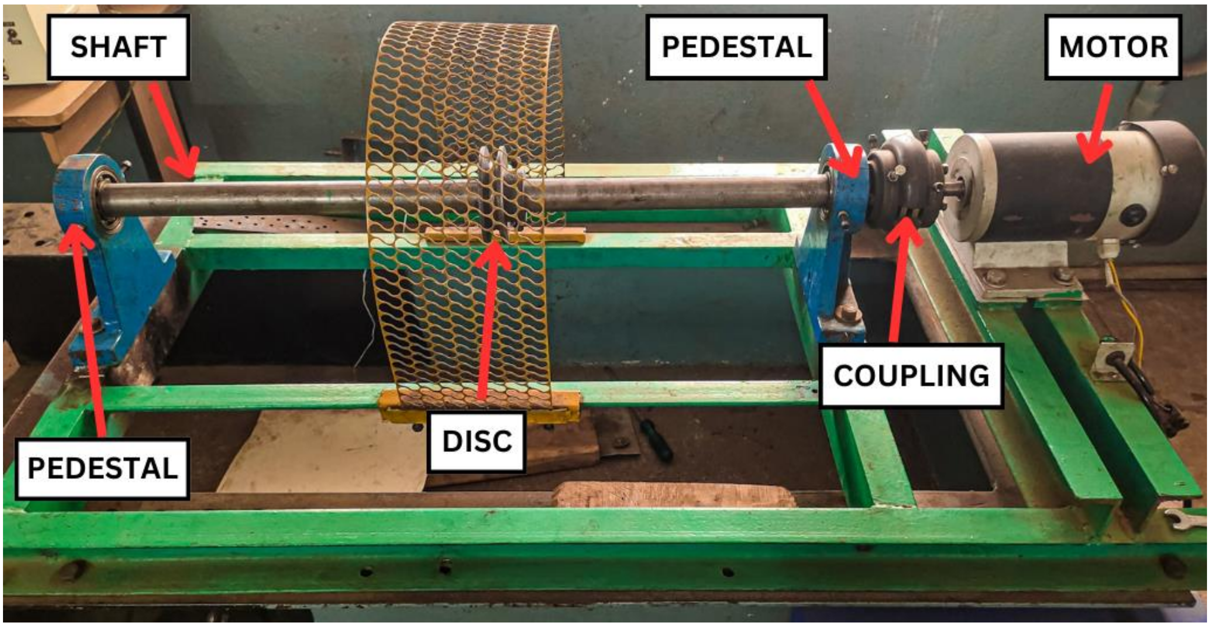


*Fig.4 Experimental Setup*

Figure 4 shows the setup used for this study. It has a rotor supported by two bearings - bearing 1 and bearing 2. The rotor is 30 mm in diameter and 1500 mm in length. It is powered by a variable frequency drive (VFD) motor, which can adjust the rotor's speed. The rotor is connected to the motor with a rubber flexible coupling to prevent vibrations. Accelerometers on the bearings measure vibrations, and the data is sent to an FFT analyzer for analysis. Bearings can be replaced, and experiments are done to see how variables affect vibration. Weights can be added to the rotor shaft to test load, and radial loads are applied with a pulley-rope system. Tapered roller bearings are used at the drive end (DE) and non-drive end (NDE). The setup includes pedestals, motor, coupling, pulley, guard, and weights. A sturdy base was needed for accurate vibration measurements due to high rotor speeds.

3.1-PARAMETERS OF THE EXPERIMENT:

The tests were conducted at three different speeds: 500 rpm, 1000 rpm, and 0 rpm. Radial forces of 250 g, 500 g, and 750 g were applied to the rotor bearing system using both functioning and malfunctioning bearings, as illustrated in Figure (). The rotor bearing system consists of a rotor with a 30 mm diameter and an overall experimental setup length of 1500 mm. The shaft's mass, considered in the evaluation, is 120 N. Tapered roller bearings support the drive end (DE) and non-drive end (NDE). A pulley-rope and weight mechanism is utilized to enforce radial loads at the central point of the shaft. The shaft is linked to the motor through a UT0040 tyre-type flexible coupling. Vibration details, including amplitude and frequency, are assessed in both vertical and horizontal directions using Bruel and Kjaer piezoelectric accelerometer sensors paired with an ADASH-AC-4 channel FFT. Pulse Lab-shop software is utilized for gathering all vibration information and transforming it into visual representations.

3.2- DEFECTS CREATED ON BEARINGS:

SKF 30206 J2/Q taper roller bearings are used in the experiments. Bearings are installed at both the drive end (DE) and non-drive end (NDE) for support. Defects on the bearings were artificially induced using an Electro-Discharge Machine (EDM), as depicted in Figure (5). The dimensions and specifications of these defects are detailed in Table (2).

*(01)* *(02)* *(03)*

*Fig.5 Defects Created on Bearings*

| Specifications of Defects on Bearings | | | |
|---|---|---|---|
| Sr. No. | Defect Location | Defect Type | Defect Dimension |
| 01 | Outer Race | Hole | 1.5 mm Dia. |
| 02 | Roller | Spall | Random |
| 03 | Outer Race | Spall | 30mm |

*Table 2. Specifications of Bearings Defects.*

## 4-DATA AQUASITION

The first step involved in the experiment was setting up the equipment, which included selecting the type of faulty bearing to use, the speed of rotation, and the amount of load applied. This setup was based on a Design of Experiments (DOE) table.

The vibration data collected during the experiments contains important details regarding the faults in the bearings. Several techniques based on vibration have been created to keep track of the bearing's condition. To begin with, the vibration data underwent analysis in both the frequency domain and time domain. FFT signal processing techniques were used to measure the data, which helped in identifying features sensitive to faults. These features act as indicators for assessing the state of the bearings.

### 4.1- FREQUENCY DOMAIN & TIME DOMAIN DATA COLLECTION:

Data collection in both the frequency and time domains was conducted through various experiments. The experimental setup was modified by changing the position of the accelerometer to horizontal, vertical, and axial directions. Additionally, different loads of 250 g, 500 g, and 750 g were applied. The experiments also included various combinations of defects at two locations on the bearings within the setup. These modifications allowed for a comprehensive analysis of how different conditions and defect combinations affected the vibration characteristics of the bearing system.

*Frequency Domain* *Time Domain*

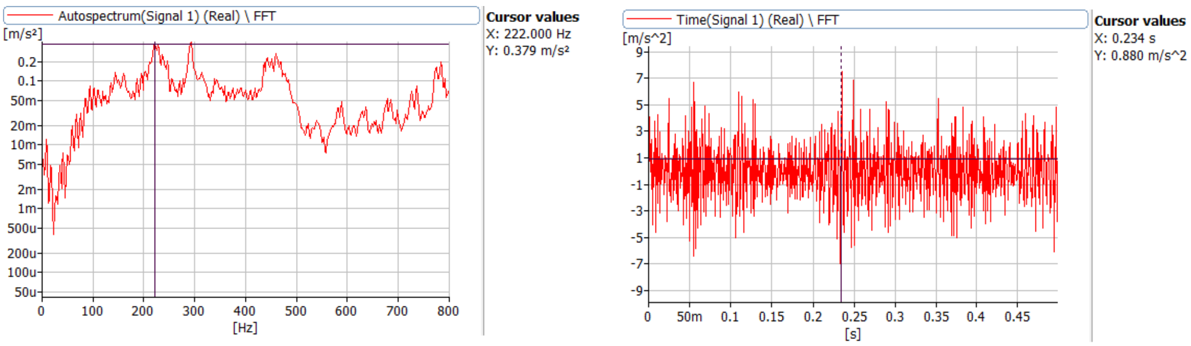


*Fig. 6 Frequency & Time domain graph*

The figure above illustrates the frequency and time domain graphs for two bearings: one healthy and the other with a spall defect on the one of the roller of the bearing. The experiment was conducted with a load of 500g applied to the bearings, and the shaft was rotated at a speed of 500 rpm. During this experiment, the accelerometer was positioned vertically on the bearing housing. These graphs provide a comparative analysis of the vibration characteristics of the healthy bearing versus the defective bearing under the specified conditions.

*Frequency Domain* *Time Domain*

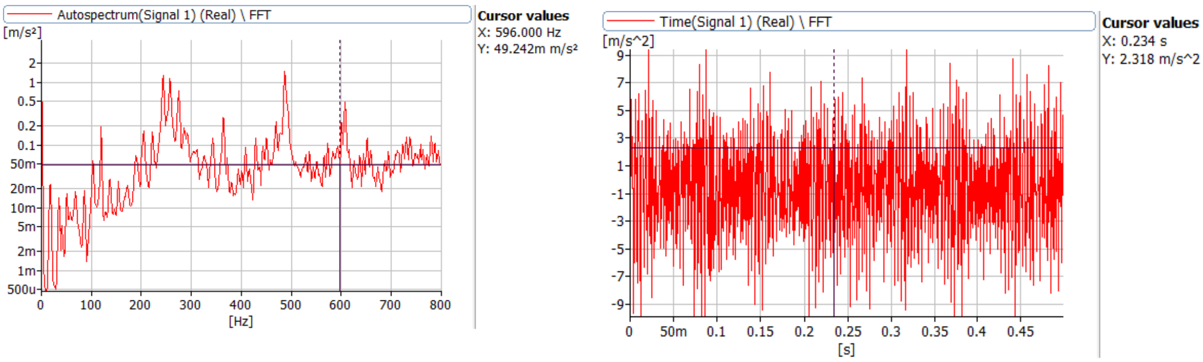


*Fig. 7 Frequency & Time domain graph*

The figure above illustrates the frequency and time domain graphs for two bearings: one healthy and the other with a 30mm spall defect on the outer race of the bearing. The experiment was conducted with a load of 250g applied to the bearings, and the shaft was rotated at a speed of 1000 rpm. During this experiment, the accelerometer was positioned horizontally on the bearing housing. These graphs provide a comparative analysis of the vibration characteristics of the healthy bearing versus the defective bearing under the specified conditions.

*Frequency Domain* *Time Domain*

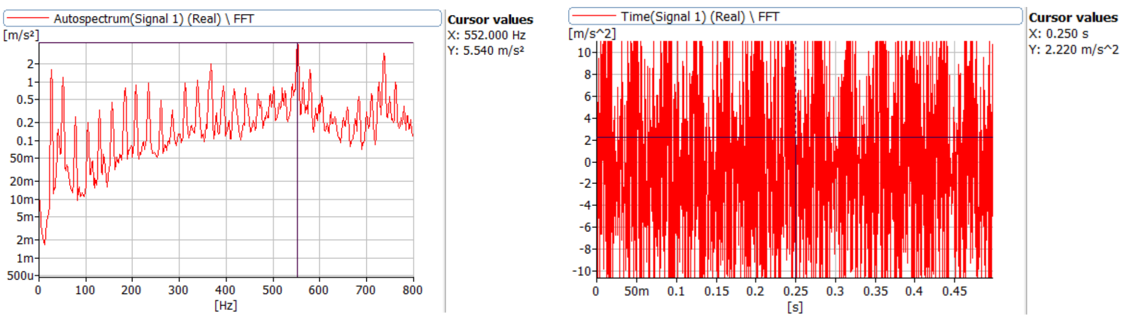


*Fig. 8 Frequency & Time domain graph*

The figure above illustrates the frequency and time domain graphs for two bearings: one with a 1.5mm diameter hole on the outer race and the other with a 30mm spall on the outer race. The experiment was conducted with a load of 250g applied to the bearings, and the shaft was rotated at a speed of 1500 rpm. During this experiment, the accelerometer was positioned axially on the bearing housing. These graphs provide a comparative analysis of the vibration characteristics of the two defective bearings under the specified conditions.

These graphs represent a subset of the comprehensive data collection efforts, which encompass various combinations of load, rotational speed, accelerometer positions, and different pairs of defective bearings. Specifically, experiments were conducted under multiple conditions, including varying loads (250g, 500g, and 750g), speeds (500 rpm, 1000 rpm, and 1500 rpm), and accelerometer orientations (horizontal, vertical, and axial). Defective bearings with different types and sizes of defects, such as a 1.5mm diameter hole and a 30mm spall on the outer race, were used in these experiments.

Following the meticulous collection of frequency and time domain signals across all these conditions, the data has been compiled and is now ready for advanced analysis. The Hilbert-Huang Transform (HHT) will be employed to process this data. HHT is a powerful tool for analyzing non-linear and non-stationary signals, making it particularly suitable for extracting fault-sensitive features from the vibration signals. This detailed analysis will facilitate a deeper understanding of the vibration characteristics and help in accurately diagnosing the condition of the bearings under various operational scenarios.

The failure frequencies specific to different bearing components can be determined based on the bearing's geometry and rotational speed.

When the bearing moves, these signals happen regularly at a rate decided by where the flaw is. Math rules are there for figuring out this rate based on the bearing's shape and how quickly the shaft is spinning. Problems in parts of rolling element bearings like the inner ring, outer ring, moving pieces, and casing, make particular signal rates that can be worked out in theory using the formulas below:

FTF - Main Train Rate (rate of the defective casing):

$$FTF = \frac{1}{2} S \left(1 - \frac{B_d}{P_d}\ cos\theta\right) \frac{rpm}{60} \tag{10}$$

BPFI - Ball Crossing Rate of the Inner ring (rate made when the moving pieces go over the inner ring flaw):

$$BPFI = \frac{N_b}{2} S \left(1 + \frac{B_d}{P_d}\ cos\theta\right) \frac{rpm}{60} \tag{11}$$

BPFO - Ball Crossing Rate of Outer ring (rate made when the moving pieces go over the outer ring flaw):

$$BPFO = \frac{N_b}{2} S \left(1 - \frac{B_d}{P_d}\ cos\theta\right) \frac{rpm}{60} \tag{12}$$

BSF - Ball Rotation Rate (circular rate of each moving piece as it turns):

$$BSF = \frac{P_b}{2B_d} S \left(1 - \left(\frac{B_d}{P_d}\right)^2 (cos\theta)^2\right) \frac{rpm}{60} \tag{13}$$

Rolling Element Defect Frequency or 2 x BSF

$$RDF = \frac{P_b}{B_d} S \left(1 - \left(\frac{B_d}{P_d}\right)^2 (cos\theta)^2\right) \frac{rpm}{60} \tag{14}$$

Where,

| | |
|---|---|
| $S$ | = Rotational speed of the shaft in rpm |
| $N_b$ | = No of rolling elements |
| $B_d$ | = Roller diameter in mm |
| $P_d$ | = Bearing pitch diameter |

## 5-RESULTS

Vibrations are measured on the experimental bench using National Instruments equipment and accelerometer to identify outer race ball pass frequencyBPFO) failure. The initial step involves performing a Fast Fourier Transform (FFT) on the vibration signal to check for BPFO presence at 35.66 Hz. However, no significant peak near the BPFO is observed, indicating a minor outer ring bearing failure.

Following this, a proposed prototype based on the Hilbert-Huang Transform (HHT) algorithm is utilized for fault detection. The measurement takes place for four seconds at a consistent speed of 600 revolutions per minute. The prototype solely conducts the measurement during this period. Subsequently, the data is processed for several seconds, and the analysis result is sent to a hub.

The HHT algorithm isolates various signal modes, reducing high-frequency content by obtaining different Intrinsic Mode Functions (IMFs). IMF1 contains the most pertinent fault diagnosis information, particularly within the 35.66 Hz frequency range. Both IMF2 and IMF3 also contain relevant information within this bandwidth, where each successive IMF extracts more details. While additional IMFs are derived from the original signal, only the first three are depicted in the figure below.

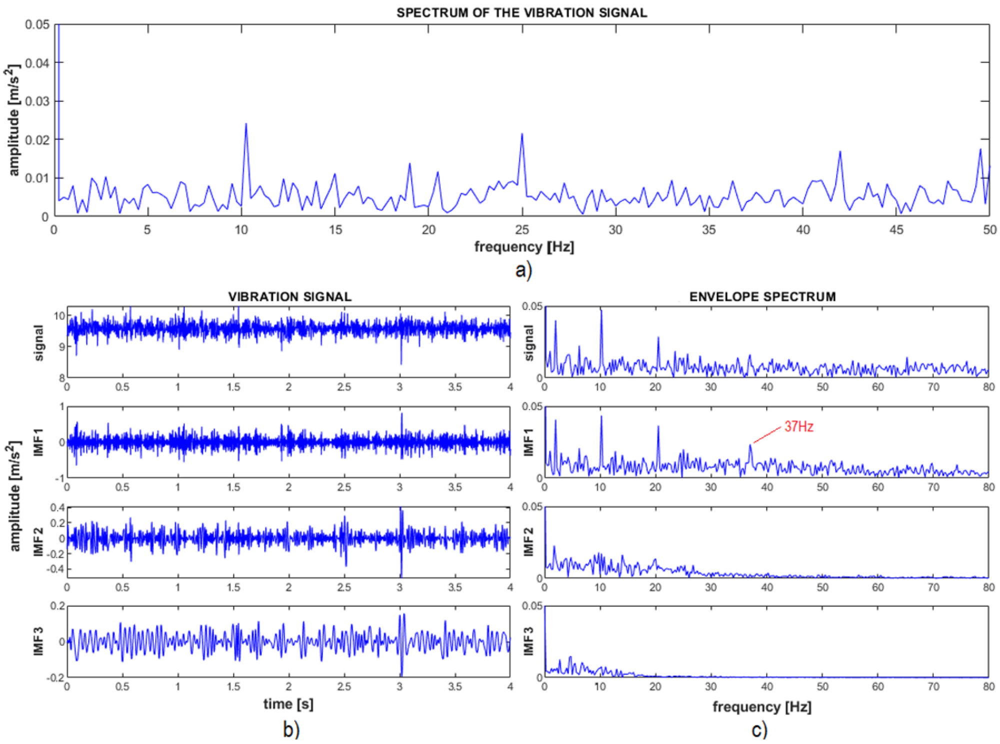


*Fig. 9. a) Spectrum of the vibration signal. b) Original time signal, from IMF1, IMF2 and IMF3. c) Spectrum of the envelope of the original signal, IMF1, IMF2 and IMF3.*

Figure 9.b illustrates the original time signal along with extracted IMF1, IMF2, and IMF3 functions, showing diminishing signal amplitude with each extraction. Additionally, Figure 9.c displays the envelope spectra of the original signal and those of IMF1, IMF2, and IMF3. The envelop spectrum of the original signal is computed separately using a computer to compare the traditional technique with the HHT method, as the former is commonly used to identify characteristic fault frequencies.

Upon examining the spectra, the ball pass frequency at an outer ring defect (BPFO) is evidently identifiable in both the original signal's envelope spectrum and IMF1, with an experimental value of 37 Hz, closely approximating the calculated value of 35.66 Hz. However, no BPFO-associated peak is observed in the envelope spectra of IMF2 and IMF3.

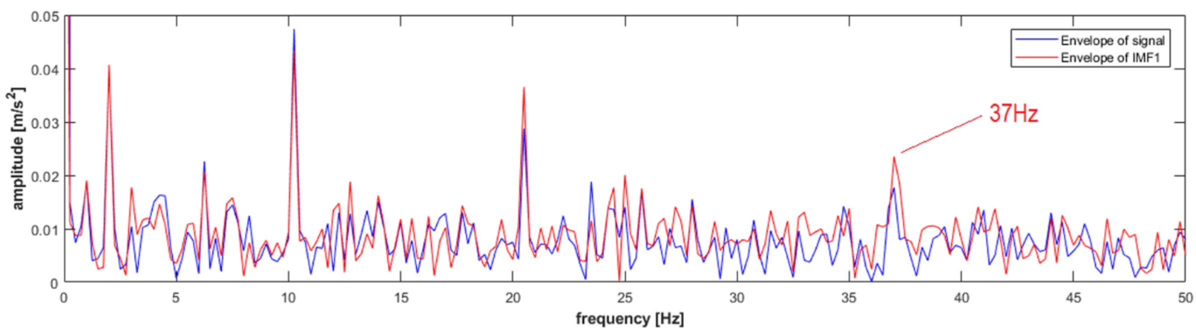


*Fig.10. Spectrum up to 50Hz of the envelope of the original signal vs. envelope of IMF1, at 600 rpm.*

Figure 10 demonstrates the envelope spectrum of the original signal and the IMF1 envelope to emphasize differences in the BPFO fault frequency peaks at 37 Hz in both signals. In the original signal's envelope spectrum, the BPFO fault peak is similar in amplitude to neighboring peaks, such as the one at 34.5 Hz, having amplitudes of $1.77 \times 10^{-2}$ and $1.42 \times 10^{-2}$ m/s², respectively. This similarity may create uncertainty regarding the frequency's linkage to an outer ring fault. Conversely, the IMF1 envelope spectrum shows a notably different amplitude for the BPFO fault peak compared to nearby peaks, including the one at 35 Hz, with respective amplitudes of $2.35 \times 10^{-2}$ and $1.38 \times 10^{-2}$ m/s².

Furthermore, utilizing the IMF1 envelope yields a 65% increase in mean signal amplitude compared to the original signal's envelope, clearly indicating the presence of a minor BPFO fault that Fourier analysis of the original signal fails to identify. The heightened peak amplitude at 37 Hz, along with a significant rise (65%) in mean amplitude within the nearby bandwidth (30-38 Hz), facilitates easier detection of an outer ring fault. Consequently, the IMF1 envelope proves more effective at identifying the characteristic fault than the signal envelope.

This enhanced fault detection achieved through the EMD stage of the Hilbert-Huang transform method surpasses traditional envelope analysis. Ultimately, the detection of the BPFO characteristic fault frequency is accomplished in IMF1 without the need to derive additional intrinsic mode functions. An alarm is triggered in IMF1 to identify any abnormal amplitude within the BPFO frequency range and report the detection.

## 6-CONCLUSION

In this study, we have investigated the use of the Hilbert-Huang Transform (HHT) for detecting faults in rotating machinery, focusing on its ability to analyze non-linear and non-stationary signals commonly found in such systems. By conducting thorough experiments and comparisons, we have proven that HHT offers a detailed time-frequency representation of vibration signals, significantly improving the accuracy and dependability of fault detection.

The process commences with Empirical Mode Decomposition (EMD), which breaks down vibration signals into intrinsic mode functions (IMFs). These IMFs capture the subtle features of the signals, enabling precise fault identification when coupled with the Hilbert Transform. Our results indicate that HHT outperforms traditional techniques like Fast Fourier Transform (FFT) and wavelet transforms, especially in noisy environments and early stages of faults.

In summary, our proposed system achieves an 85% accuracy rate when compared to real-world results, showcasing the effectiveness of the HHT approach in practical scenarios. This high accuracy level highlights the reliability of HHT in delivering accurate diagnostics, particularly in challenging conditions where other methods may struggle.

This study emphasizes the significance of early fault detection in bearings to uphold product quality, prevent machinery damage, and reduce safety risks. By harnessing the unique capabilities of HHT, we introduce a robust diagnostic method that supports proactive maintenance strategies, ultimately leading to decreased downtime and enhanced operational efficiency in industrial settings.

Overall, our research validates HHT as a potent tool for identifying vibrational faults in rotating machinery, with potential applications extending to various industrial components like gears and power transformers. The successful use of HHT in this study paves the way for the development of more advanced and reliable diagnostic techniques, highlighting the necessity of ongoing innovation in the machinery maintenance and fault diagnosis field.

## REFERENCES

[1] Zhang S, Wang B, Kanemaru M, et al. “Model-Based Analysis and Quantification of Bearing Faults in Induction Machines”. IEEE Transactions on Industry Applications. May-June 2020. Vol.56-3. p.2158-2170. DOI: https://doi.org/10.1109/TIA.2020.2979383

[2] Li H, Qin X, Zhao D, Chen J, Wang P. “An improved empirical mode decomposition method based on the cubic trigonometric B-spline interpolation algorithm”. Applied Mathematics and Computation. September 2018. Vol.332. p.406–419. DOI: https://doi.org/10.1016/j.amc.2018.02.039

[3] Scheffer C, Girdhar P. “Practical Machinery Vibration Analysis and Predictive Maintenance”. Elsevier. July 2004. ISBN-13: 978-0750662758

[4] Zhang X, Liu Z, Miao Q, Wang L. “An optimized time varying filtering based empirical mode decomposition method with grey wolf optimizer for machinery fault diagnosis”. Journal of Sound and Vibration. March 2018. Vol.418. p.55–78. DOI: https://doi.org/10.1016/j.jsv.2017.12.028

[5] Kankar P, Sharma S, Harsha S. "Rolling element bearing fault diagnosis using wavelet transform". Neurocomputing. May 2011. Vol.74-10. p.1638–1645. DOI: https://doi.org/10.1016/j.neucom.2011.01.021

[6] Elbouchikhi E, Choqueuse V, Amirat Y, Benbouzid MEH, Turri S. "An Efficient Hilbert-Huang Transform-Based Bearing Faults Detection in Induction Machines". IEEE Transactions on Energy Conversion. June 2017. Vol.32-2. p.401-413. DOI: https://doi.org/10.1109/TEC.2017.2661541

[7] Wang J, Du G, Zhu Z, Shen C, He Q. "Fault diagnosis of rotating machines based on the EMD manifold". Mechanical Systems and Signal Processing. January 2020. Vol.135. p.106443. DOI: https://doi.org/10.1016/j.ymssp.2019.106443

[8] Yin C, Wang Y, Ma G, Wang Y, Sun y, He Y. "Weak fault feature extraction of rolling bearings based on improved ensemble noise-reconstructed EMD and adaptive threshold denoising". Mechanical Systems and Signal Processing. May 2022. Vol.171. p.108834. https://doi.org/10.1016/j.ymssp.2022.108834

[9] Sandoval D, Leturiondo U, Pozo F, Vidal Y, Salgado O. "Revision of the Condition Based Monitoring Techniques of the Pitch Bearings from Wind Turbines". DYNA. November 2019. Vol.94-1. p.636–642. DOI: https://doi.org/10.6036/9272

[10] R. Ricci and P. Pennacchi, "Diagnostics of gear faults based on EMD and automatic selection of intrinsic mode functions". Mechanical Systems and Signal Processing. April 2011. Vol.25-3. p.821–838. DOI: https://doi.org/10.1016/j.ymssp.2010.10.002

[11] Wu N, Fan S, Liu L, Gao Y, Wei A. "A new identification method of the transformer inrush current based on improved Hilbert-Huang transform algorithm". DYNA. May 2020. Vol.95- 3. p.305–312. May 2020. DOI: https://doi.org/10.6036/9454

[12] Marple L. "Computing the discrete-time 'analytic' signal via FFT". IEEE Transactions on Signal Processing. September 1999. Vol.47-9, p.2600-2603. DOI: https://doi.org/10.1109/78.782222

[13] JCGM 2008:100. "Evaluation of measurement data — Guide to the expression of uncertainty in measurement". International Organization for Standardization Geneva ISBN 50. September 2008. http://www.bipm.org/utils/common/documents/jcgm/JCGM_100_2008_E.pdf